

Smooth Quantum Hydrodynamic Model vs. NEMO Simulation of Resonant Tunneling Diodes

Carl L. Gardner
Department of Mathematics and Statistics
Arizona State University
Tempe, AZ 85287

Gerhard Klimeck*
Jet Propulsion Laboratory
California Institute of Technology
Pasadena, CA 91109
and
Network for Computational Nanotechnology
School of Electrical and Computer Engineering
Purdue University
West Lafayette, IN 47907

Christian Ringhofer
Department of Mathematics and Statistics
Arizona State University
Tempe, AZ 85287

Keywords: resonant tunneling diode, quantum hydrodynamic model, NEMO.

*The NEMO work described in this article was carried out in part at the Jet Propulsion Laboratory, California Institute of Technology under a contract with the National

Abstract

The smooth quantum hydrodynamic model is an extension of the classical hydrodynamic model for semiconductor devices which can handle in a mathematically rigorous way the discontinuities in the classical potential energy which occur at heterojunction barriers in quantum semiconductor devices. Smooth QHD model simulations of the current-voltage curves of resonant tunneling diodes are presented which exhibit negative differential resistance—the experimental signal for quantum resonance effects—and are compared with the experimentally verified current-voltage curves predicted by the simulator NEMO, which uses a non-equilibrium Green function method.

1 Introduction

In this investigation we will compare simulations of a single barrier structure and of two resonant tunneling diodes (RTDs) using the smooth quantum hydrodynamic (QHD) model and the simulator NEMO, which uses a non-equilibrium Green function method. We will view the NEMO method as experimentally verified [1], and contrast the negative differential resistance in the current-voltage curves predicted by NEMO for the RTDs with that predicted by the smooth QHD model.

The smooth QHD model will first be calibrated against NEMO on a single barrier structure, and then the RTD simulations will be performed with the calibrated parameters. We have attempted to make the physics going into the two different approaches as nearly the same as possible. However it is impossible to make an exact comparison, since NEMO assumes the contacts are thermal equilibrium reservoirs (at ambient temperature T_0) and that the quantum regions of the device are non-equilibrium (so that temperature cannot be defined), while QHD—as a fluid dynamical approximation—assumes the whole device is everywhere locally “near” thermal equilibrium, and that the electron gas temperature T relaxes to $dT/dx = 0$ at the outer boundaries of the contacts (the temperature need not relax to T_0).

We are not recommending that the design space of a RTD be explored with the QHD model; that should be done with NEMO. However, once calibrated, the QHD model gives qualitatively correct results, and the QHD

Aeronautics and Space Administration. This material is also based upon work supported by the National Science Foundation under Grant No. EEC-0228390.

model may be used for simulating RTDs with “nearby” parameters and for similar RTDs that make up one component of compound devices, as well as for simulating quantum effects in field effect transistors.

2 Smooth QHD Model

Quantum transport effects including electron or hole tunneling through potential barriers and charge buildup in quantum wells can be incorporated into the hydrodynamic description of charge propagation in semiconductor devices. Refs. [2, 3, 4] present an extension of the classical hydrodynamic model which can handle in a mathematically rigorous way the discontinuities in the classical potential energy which occur at heterojunction barriers in quantum semiconductor devices. This smooth quantum hydrodynamic model is valid to all orders of $\hbar^2/(mT_0l^2)$ (where m is the effective mass of electrons or holes, and l is a typical length scale for the problem) and to first order in the classical potential energy.

The smooth QHD equations have the same form as the classical hydrodynamic equations:

$$\frac{\partial n}{\partial t} + \frac{\partial}{\partial x_i}(nu_i) = 0 \quad (1)$$

$$\frac{\partial}{\partial t}(mnu_j) + \frac{\partial}{\partial x_i}(mnu_iu_j - P_{ij}) = -n\frac{\partial V}{\partial x_j} - \frac{mnu_j}{\tau_p} \quad (2)$$

$$\frac{\partial W}{\partial t} + \frac{\partial}{\partial x_i}(u_iW - u_jP_{ij} + q_i) = -nu_i\frac{\partial V}{\partial x_i} - \frac{(W - \frac{3}{2}nT_0)}{\tau_w} \quad (3)$$

where n is the electron density, u_i is the velocity, m is the effective electron mass, P_{ij} is the stress tensor, V is the potential energy, W is the energy density, and q_i is the generalized heat flux. Boltzmann’s constant k_B is set equal to 1. Indices i, j equal 1, 2, 3, and repeated indices are summed over. Electron scattering is modeled by the standard relaxation time approximation, with momentum and energy relaxation times τ_p and τ_w .

The stress tensor and energy density are

$$P_{ij} = -nT\delta_{ij} - \frac{\hbar^2n}{4mT_0}\frac{\partial^2\bar{V}}{\partial x_i\partial x_j} \quad (4)$$

$$W = \frac{3}{2}nT + \frac{1}{2}mnu^2 + \frac{\hbar^2n}{8mT_0}\nabla^2\bar{V} \quad (5)$$

where T is the temperature of the electron gas and the “quantum” potential \bar{V} is given by ($\beta = 1/T_0$)

$$\bar{V}(\beta, \mathbf{x}) = \int_0^\beta \frac{d\beta'}{\beta} \left(\frac{\beta'}{\beta} \right)^2 \int d^3x' \left(\frac{2m\beta}{\pi(\beta - \beta')(\beta + \beta')\hbar^2} \right)^{3/2} \times \exp \left\{ -\frac{2m\beta}{(\beta - \beta')(\beta + \beta')\hbar^2} (\mathbf{x}' - \mathbf{x})^2 \right\} V(\mathbf{x}'). \quad (6)$$

The generalized heat flux

$$\mathbf{q} = -\kappa \nabla T - \frac{\hbar^2 n}{8m} \nabla^2 \mathbf{u} \quad (7)$$

includes both classical and quantum effects and is derived in Ref. [5] by a Chapman-Enskog expansion. The quantum contribution to the heat flux is necessary for internal consistency of the QHD model. The generalized heat flux incorporates the most important effects of the higher moments of the Wigner-Boltzmann transport equation which are omitted in the fluid dynamical approximation.

Scattering is turned off in the smooth QHD simulations in the quantum region of the devices (spacers, barriers, and wells), while in the contacts scattering is crucial in order that the electron gas relaxes back to the ambient temperature at the device boundaries. The hydrodynamic approximation only allows the electrons in the contacts to cool down or heat up to near ambient temperature over a length scale on the order of 100 nm (see Fig. 11) for the RTDs analyzed here. Thinner contacts may be used, but then a direct comparison with NEMO (with its contacts at T_0) is not possible.

We model the relaxation times τ_p and τ_w in the contacts by modified Baccarani-Wordeman models [6, 7]

$$\tau_p = m\mu_{n0} \frac{T_0}{T}, \quad \tau_w = \frac{\tau_p}{2} \left(1 + \frac{\frac{3}{2}T}{\frac{1}{2}mv_s^2} \right) \quad (8)$$

and the coefficient κ by

$$\kappa = \kappa_0 \mu_{n0} n T_0 \quad (9)$$

where μ_{n0} is the low-field electron mobility, v_s is the electron saturation velocity, and $\kappa_0 > 0$ is a phenomenological constant.

The transport equations (1)–(3) are coupled to Poisson’s equation for the electrostatic potential energy

$$\nabla \cdot (\epsilon \nabla V_P) = e^2(N - n) \quad (10)$$

where ϵ is the dielectric constant, $e > 0$ is the electronic charge, and N is the density of donors. The total potential energy V consists of two parts, one from Poisson’s equation V_P and the other from the potential barriers V_B :

$$V = V_B + V_P. \quad (11)$$

V_B has a step function discontinuity at potential barriers.

To derive the stress tensor and energy density, we constructed a “quantum Maxwellian” density matrix as an $O(\beta V)$ solution to the Bloch equation. Then using the momentum-shifted quantum Maxwellian, we took moments of the Wigner-Boltzmann transport equation to derive the smooth QHD equations [2].

There are two contributions to the quantum potential \bar{V} : the double barrier potential and the self-consistent electrostatic potential from Poisson’s equation. Note that second derivatives of \bar{V} appear in the stress tensor and energy density, which then are differenced in the smooth QHD transport equations. Thus we compute

$$\bar{V}'' = \bar{V}_B'' + \bar{V}_P''. \quad (12)$$

\bar{V}_B'' is just computed once since it only depends on the barriers and not on the applied voltage or state variables (n , u , T , V_P). In computing \bar{V}_P'' , we first use Poisson’s equation to obtain

$$\begin{aligned} \bar{V}_P''(\beta, x) = & \frac{e^2}{\epsilon} \int_0^\beta \frac{d\beta'}{\beta} \left(\frac{\beta'}{\beta}\right)^2 \int dx' \left(\frac{2m\beta}{\pi(\beta - \beta')(\beta + \beta')\hbar^2}\right)^{3/2} \times \\ & \exp\left\{-\frac{2m\beta}{(\beta - \beta')(\beta + \beta')\hbar^2}x'^2\right\} (N(x' + x) - n(x' + x)). \end{aligned} \quad (13)$$

The convolution (13) can be computed efficiently using discrete Fourier transform algorithms.

In order to calibrate the smooth QHD model, first we simulate a single $\text{Al}_{0.3}\text{Ga}_{0.7}\text{As}$ barrier diode at 300 K (see Fig. 1). The barrier height is equal to 280 meV. The diode consists of n^+ source (at the left) and drain (at the

right) regions with the doping density $N = 10^{18} \text{ cm}^{-3}$, and an n channel with $N = 5 \times 10^{15} \text{ cm}^{-3}$. The barrier is 5 nm wide, and there are 5 nm spacers between the barrier and the contacts. A good fit with NEMO is obtained if $\mu_{n0} = 1000 \text{ cm}^2/(\text{V s})$ in the contacts.

Then we simulate two GaAs resonant tunneling diodes with $\text{Al}_{0.3}\text{Ga}_{0.7}\text{As}$ double barriers at 300 K. The barrier height is equal to 280 meV. The diode consists of n^+ source (at the left) and drain (at the right) regions with the doping density $N = 10^{18} \text{ cm}^{-3}$, and an n channel with $N = 5 \times 10^{15} \text{ cm}^{-3}$. The barriers are 2.5 nm wide, and the quantum well between the barriers is 5 nm wide in the first (“medium well”) case, and 3.5 nm wide in the second (“thin well”) case. Both RTD devices have 5 nm spacers between the barriers and the high doping contacts.

For the smooth QHD simulations we take $m = 0.063 m_e$, $\mu_{n0} = 1000 \text{ cm}^2/(\text{V s})$ or $2000 \text{ cm}^2/(\text{V s})$ in the contacts, $v_s = 1.5 \times 10^7 \text{ cm/s}$, and $\epsilon = 12.9$. The effective mass is taken here to be constant throughout the device. We use the canonical value $\kappa_0 = 2.5$ for the resonant tunneling diodes; for the single barrier device, $\kappa_0 = 0.5$ gives better agreement with NEMO. Our numerical experience with the classical hydrodynamic model and with the QHD model applied to classical or single barrier devices indicates that a low value of $\kappa_0 \approx 0.5$ is more physical (suggesting that higher moment effects are not very important in these devices), while for RTDs, a higher value of $\kappa_0 \approx 2.5$ is more physical (suggesting that higher moment effects are very important in these devices).

All the assumptions for the smooth QHD model are also made for NEMO, except that v_s and κ_0 do not appear in NEMO. Heat conduction—which is proportional to κ_0 —represents, as mentioned above, the effects of higher moments omitted in the QHD approximation. The QHD simulations are not very sensitive to the value of v_s .

Figs. 2 and 3 display the experimental signal of quantum resonance—negative differential resistance (NDR), a region of the current-voltage (I-V) curve where the current *decreases* as the applied voltage is increased—for the smooth QHD model for $\mu_{n0} = 1000 \text{ cm}^2/(\text{V s})$ and, for the sake of comparison, for $\mu_{n0} = 2000 \text{ cm}^2/(\text{V s})$.

Fig. 4 demonstrates that NDR is *not* due to unequal relaxation times in the smooth QHD simulations.

3 NEMO Simulations

The need for a quantitative resonant tunneling device modeling tool prompted a device modeling project at the Central Research Laboratory of Texas Instruments (which transferred to Raytheon Systems in 1997). NEMO was developed as a general purpose quantum mechanics-based 1D device design and analysis tool from 1993–97. The tool is available to US researchers by request on the NEMO web site [8]. NEMO is based on the non-equilibrium Green function (NEGF) approach, which allows a fundamentally sound inclusion of the required physics: band structure, scattering, and charge self-consistency. The theoretical approach is documented in Refs. [9, 10] while some of the major simulation results are documented in Refs. [11, 12, 13, 14, 15, 16]. NEMO development is presently continued [8] at the Jet Propulsion Laboratory towards the modeling of light detection and emission devices.

Generally NEMO simulations are based on a resolution of every atomic layer in a heterostructure. A typical unit cell in GaAs is 0.2833 nm to properly resolve heterostructures and represent the underlying bandstructure dispersion. Typical room temperature simulations are performed using advanced bandstructure models such as sp3s* nearest neighbor, sp3s* second-nearest neighbor, or sp3d5s* nearest neighbor models, to properly include effects of non-parabolicity, multiple conduction band valleys, and conduction-valence band wrapping, even for purely electronic conduction devices [12, 13]. Purely single band simulations have been found to be appropriate to model the peak current for RTDs when the correct effective mass is used for the barrier material [11]. However, the single band model typically fails to represent the valley current and the second turn-on of realistic RTDs [11, 12, 13] in room temperature experiments. This failure is typically not due to lack of scattering in the RTD, but due to the lack of appropriate representation of high energy carrier transport due to the simplistic bandstructure model. Only for low temperature experiments have single band models have been shown to properly model the valley current when interface roughness scattering and polar optical phonon scattering are included [9, 16]. For the sake of comparison with the currently implemented QHD model we have simplified the NEMO simulations to be based on a single constant effective mass. This approximation will result in an approximately 75% increased current density in the structures considered here compared to the use of the appropriate effective mass in the barriers.

The medium well structure simulated in NEMO consists of the central

resonant tunneling diode described by 9 monolayer ≈ 2.5 nm $\text{Al}_{0.3}\text{Ga}_{0.7}\text{As}$ barriers and a 18 monolayer ≈ 5.1 nm GaAs well. It is clad symmetrically by 18 monolayers of low doping GaAs spacer of $5 \times 10^{15} \text{ cm}^{-3}$ and 30 nm high doping contacts of 10^{18} cm^{-3} . The thin quantum well RTD consists of 12 monolayers ≈ 3.4 nm. The NEMO simulations shown here are based on a single band single effective mass model, $m_{\text{GaAs}} = m_{\text{AlGaAs}} = 0.063 m_e$ and $\Delta E_c = 278$ meV. The potential in these simulations is based on a self-consistent Hartree potential and includes the exchange energy within the LDA approximation. Only a small relaxation potential [11] $\eta = \hbar/(2\tau) = 0.1$ meV is included in the contacts to minimize any artifacts in the charge distribution in the contacts and enable a simplified comparison with the QHD model.

The thin barriers push the current densities to very high values for GaAs/AlGaAs structures. The NEMO simulations shown in this investigation include the recently developed semi-classical transport models that couple NEGF to a drift-diffusion approach [17]. A uniform, doping-independent mobility of $1000 \text{ cm}^2/(\text{V s})$ is used in the contacts. The traditional NEGF approach corresponds to an infinite mobility in the contacts. The current density in the 5.1 nm quantum well case (Fig. 2) is large enough such that the peak current density is reduced from 555 kA/cm^2 to 454 kA/cm^2 . The thin quantum well RTD (Fig. 3) pushes the resonance higher in energy and overall increases the current density to 1010 kA/cm^2 . A uniform mobility of $1000 \text{ cm}^2/(\text{V s})$ reduces the overall current density in the device to the peak current density of 764 kA/cm^2 as shown in Fig. 3. This is a significant peak current reduction, while the peak voltage is only slightly changed. This indicates that the details of the potential distribution modify the current flow significantly.

The I-V peak position occurs roughly when the central RTD resonance is lowered under the emitter subband by the applied bias. For the medium well RTD at zero bias, the central resonance is predicted at approximately 105–108 meV. That energy includes a built-in potential of about 30 meV above the contact band edge due to the low doping in the central region. Assuming a semiclassical charge distribution in the contacts and zero charge in the central RTD, NEMO predicts a current peak at about 210 mV (not shown here). Including Hartree self-consistency linearizes the I-V curve and pushes the peak to a higher voltage [11, 13] at 250 mV.

4 Comparison and Conclusion

In comparing the medium well and the thin well RTD I-V curves, note that in NEMO the peak voltage moves from 0.3 volts to 0.4 volts as the well narrows. This shift in the peak voltage is reproduced by the smooth QHD simulations, where the peak voltage moves from 0.2 volts to 0.3 volts. Note also that the qualitative shapes of the current resonances are similar in the two different approaches.

If we view the RTD NEMO simulations as an experimentally verified standard [1], we conclude that the hydrodynamic model predicts current densities that are in excellent agreement. However the peak voltage is too low due to the differences in modeling the contacts and to the QHD modification of charge buildup in the quantum well (see Figs. 6, 8, and 10, and the discussion below).

Although it is difficult to compare conduction band energies and electron densities at critical bias points—both because the I-V curves for the two different approaches are different and because the smooth QHD simulations require long contacts for the electron gas to reach ambient temperature, nonetheless there is reasonable agreement between the sets of curves shown in Figs. 5–10. However, note the following differences: In Fig. 5, the QHD simulations show a significant potential drop in the extended contact regions, while the NEMO simulations show an almost flat conduction band edge. In Figs. 6 and 8, the NEMO simulations show significant charge accumulation inside the quantum well, which results in the linearization of the I-V curve. And in comparing Fig. 10 with Figs. 6 and 8, the NEMO simulation now shows little charge accumulation in the quantum well. The device is in the valley current regime (the off state), and charge is expected to be negligible.

It must be emphasized that QHD is an approximation, both in that it is a fluid dynamical truncation of the moment expansion of the Wigner-Boltzmann transport equation, and in that it is an quantum approximation linear in the potential energy V . Linearizing in V does modify [18] to some extent the charge buildup in the quantum well of the RTD (see Figs. 6, 8, and 10). However the QHD model does exhibit tunneling for single barriers and negative differential resistance for double barriers.

The modeling of resonant tunneling diodes has been studied intensively over the past 25 years. The position and amplitude of the main resonant peak has generally been successfully modeled with simple effective mass band models based on a self-consistent Poisson-Schrödinger equation solution. The

QHD approach presented here also demonstrates this capability. From an experimental point of view it is imperative to reduce the valley current for analog as well as digital applications. The peak current is carried through a resonant tunneling process where the resonance width is wider than the injecting energy range (Fermi level). When the resonance is pulled out of the range of injection energies the current is carried by off-resonant processes. Coherent off-resonant current can be exponentially damped by increasing the barrier widths without affecting the resonant peak current. Practically relevant RTDs in the AlGaAs or InGaAs/InAlAs/InP material system are therefore typically 5 nm in width. However, even though the barriers are thick the best peak to valley ratios have been around 80 with typical values around 10. Before the NEMO project the origin of this valley current was attributed to inelastic scattering. NEMO simulations however showed that not inelastic scattering but thermionic emission through excited states is the key ingredient to the understanding of the valley current in room temperature RTDs [12, 13]. Inelastic scattering is only the dominant effect in low temperature experiments in the AlGaAs and InGaAs/InAlAs/InP material system.

The devices studied here have barrier thicknesses of 2.5 nm, with a barrier height of 280 meV and an effective mass of 0.063. This corresponds roughly speaking to an $\text{Al}_{0.22}\text{Ga}_{0.78}\text{As}$ barrier with a barrier height of 204 meV and an effective mass of 0.084. These correspond to very thin and shallow barriers allowing for a significant *coherent* off-resonant current. The NEMO simulations for these devices show that the valley current is carried solely through off-resonant current tunneling without any scattering in the central RTD or the emitter quasi-bound states. Also no significant bandstructure effects are visible in this valley current. The QHD method succeeds in predicting the same valley current for these particular devices, since the valley current is a purely coherent off-resonant process due to the thin barriers.

What we see from the comparisons presented above is that the QHD model needs a better model for the contacts, and a more sophisticated model for heat flux (which incorporates higher moment effects) in the quantum region. The QHD fluid approximation here treats a single electron gas that has a macroscopic positive velocity for the 1D RTDs and single barrier device. However two electron gases (hot electrons from the source and cold electrons from the drain) could be simulated—including interactions between them—and would perhaps give better results. Work on these issues and on a more detailed comparison of the two models on more realistic devices, including

two effective masses and non-parabolic bands, is in progress.

References

- [1] The NEMO simulations shown here are extremely oversimplified to match the parameter space explored with the QHD model. In particular, a single material independent mass is used in the NEMO simulations as well as the QHD simulations. Furthermore effects such as complex band-wrapping, band non-parabolicity, and multiple conduction band valleys that would typically be treated within NEMO are neglected here. NEMO simulations have shown in the past that these effects are of utmost importance for the quantitative modeling of resonant tunneling diodes at room temperature.
- [2] C. L. Gardner and C. Ringhofer, “Smooth quantum potential for the hydrodynamic model,” *Physical Review E*, vol. 53, pp. 157–167, 1996.
- [3] C. L. Gardner and C. Ringhofer, “Approximation of thermal equilibrium for quantum gases with discontinuous potentials and application to semiconductor devices,” *SIAM Journal on Applied Mathematics*, vol. 58, pp. 780–805, 1998.
- [4] C. L. Gardner and C. Ringhofer, “Dispersive/Hyperbolic Hydrodynamic Models for Quantum Transport (in Semiconductor Devices),” in *Dispersive Transport Equations and Multiscale Models*, IMA Volumes in Mathematics and its Applications, Volume 136, pp. 91–106. New York: Springer-Verlag, 2003.
- [5] C. L. Gardner and C. Ringhofer, “The Chapman-Enskog expansion and the quantum hydrodynamic model for semiconductor devices,” *VLSI Design*, vol. 10, pp. 415–435, 2000.
- [6] G. Baccarani and M. R. Wordeman, “An investigation of steady-state velocity overshoot effects in Si and GaAs devices,” *Solid State Electronics*, vol. 28, pp. 407–416, 1985.
- [7] C. L. Gardner, “Shock waves in the hydrodynamic model for semiconductor devices,” in *Semiconductors*, IMA Volumes in Mathematics and its Applications, Volume 59, pp. 123–134. New York: Springer-Verlag, 1993.

- [8] Raytheon no longer distributes the NEMO code. However US researchers that conduct research under a government contract and require NEMO can request the software based on a government use license from JPL. Details can be found on the NEMO web page at JPL: <http://hpc.jpl.nasa.gov/PEP/gekco/nemo/>.
- [9] R. K. Lake, G. Klimeck, R. C. Bowen, and D. Jovanovic, "Single and multiband modeling of quantum electron transport through layered semiconductor devices," *Journal of Applied Physics*, vol. 81, pp. 7845–7869, 1997.
- [10] R. K. Lake, G. Klimeck, R. C. Bowen, D. Jovanovic, D. K. Blanks, and M. Swaminathan, "Quantum transport with band-structure and Schottky contacts," *Physica Status Solidi B*, vol. 204, pp. 354–357, 1997.
- [11] G. Klimeck, R. K. Lake, R. C. Bowen, W. R. Frensley, and T. S. Moise, "Quantum device simulation with a generalized tunneling formula," *Applied Physics Letters*, vol. 67, pp. 2539–2541, 1995.
- [12] G. Klimeck, T. Boykin, R. C. Bowen, R. K. Lake, D. K. Blanks, T. S. Moise, Y. C. Kao, and W. R. Frensley, in *1997 55th Annual Device Research Conference Digest*, p. 92. IEEE, 1997.
- [13] R. C. Bowen, G. Klimeck, R. K. Lake, W. R. Frensley, T. S. Moise, "Quantitative simulation of a resonant tunneling diode," *Journal of Applied Physics*, vol. 81, pp. 3207–3213, 1997.
- [14] R. K. Lake, G. Klimeck, R. C. Bowen, C. Fernando, T. S. Moise, Y. C. Kao, "Interface roughness, polar optical phonons, and the valley current of a resonant tunneling diode," *Superlattices and Microstructures*, vol. 20, pp. 279–285, 1996.
- [15] R. K. Lake, G. Klimeck, and D. K. Blanks, "Interface roughness and polar optical phonon scattering in $\text{In}_{0.53}\text{Ga}_{0.47}\text{As}/\text{AlAs}/\text{InAs}$ RTDs," *Semiconductor Science and Technology*, vol. 13, pp. A163–A164, 1998.
- [16] G. Klimeck, R. K. Lake, and D. K. Blanks, "Role of interface roughness scattering in self-consistent resonant-tunneling-diode simulations," *Physical Review B*, vol. 58, pp. 7279–7285, 1998.

- [17] G. Klimeck, “Quantum and semi-classical transport in RTDs in NEMO 1-D,” *Journal of Computational Electronics*, vol. 2, pp. 177–182, 2003.
- [18] C. L. Gardner and C. Ringhofer, unpublished comparison of the quantum Maxwellian and numerical solutions of the Bloch equation.

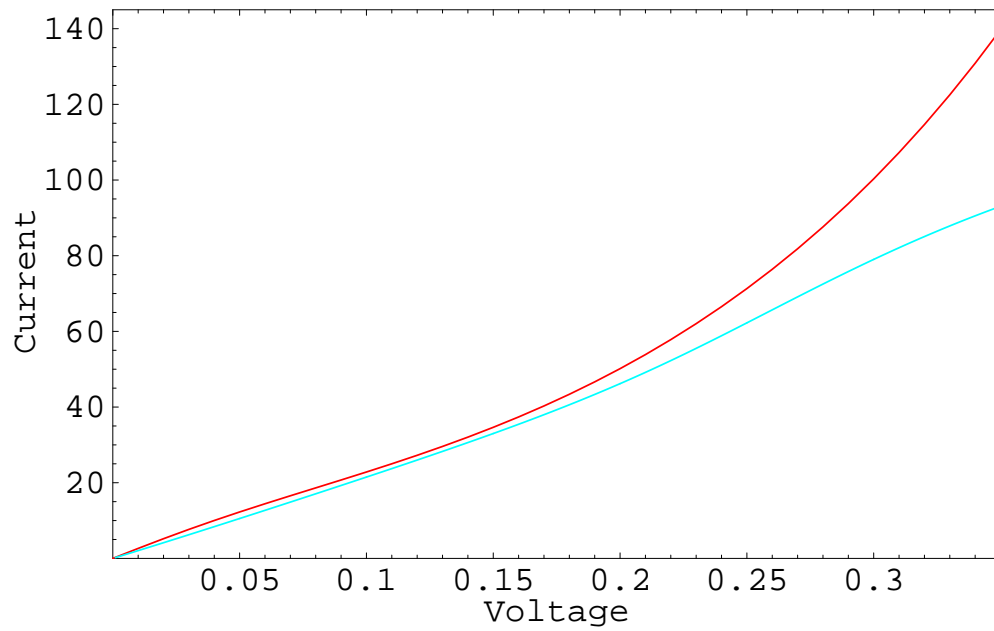


Figure 1: Current in kA/cm² vs. applied bias in volts for the single 5 nm barrier diode: NEMO (red, dark), smooth QHD with $\mu_{n0} = 1000 \text{ cm}^2/(\text{V s})$ (cyan, light) in the contacts.

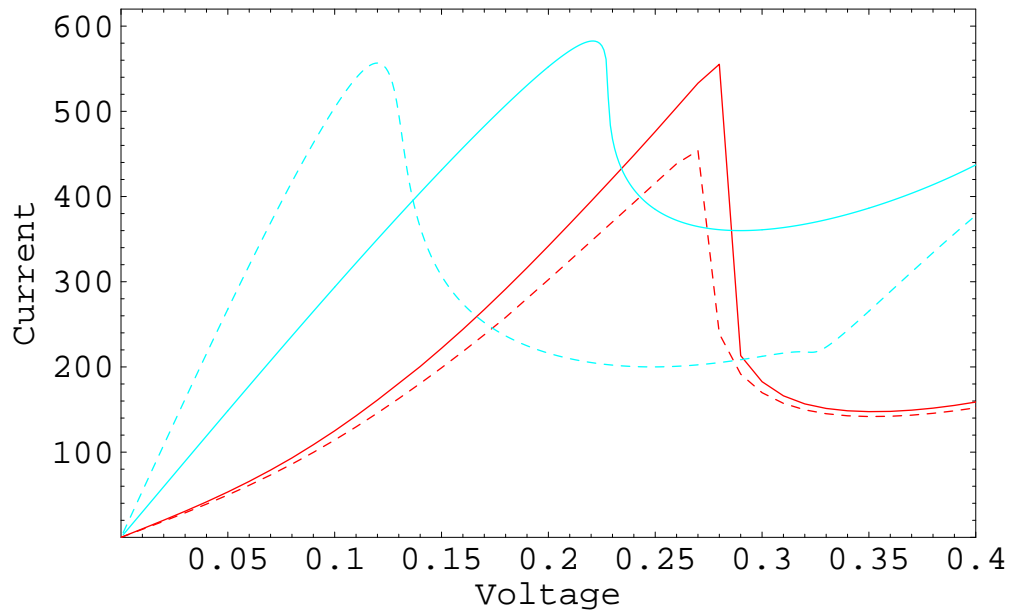


Figure 2: Current in kA/cm^2 vs. applied bias in volts for the medium (5 nm) well RTD: NEMO (red, dark), NEMO plus drift-diffusion (dotted red, dotted dark) in the contacts, smooth QHD with $\mu_{n0} = 1000 \text{ cm}^2/(\text{V s})$ (cyan, light) in the contacts, smooth QHD with $\mu_{n0} = 2000 \text{ cm}^2/(\text{V s})$ (dotted cyan, dotted light) in the contacts.

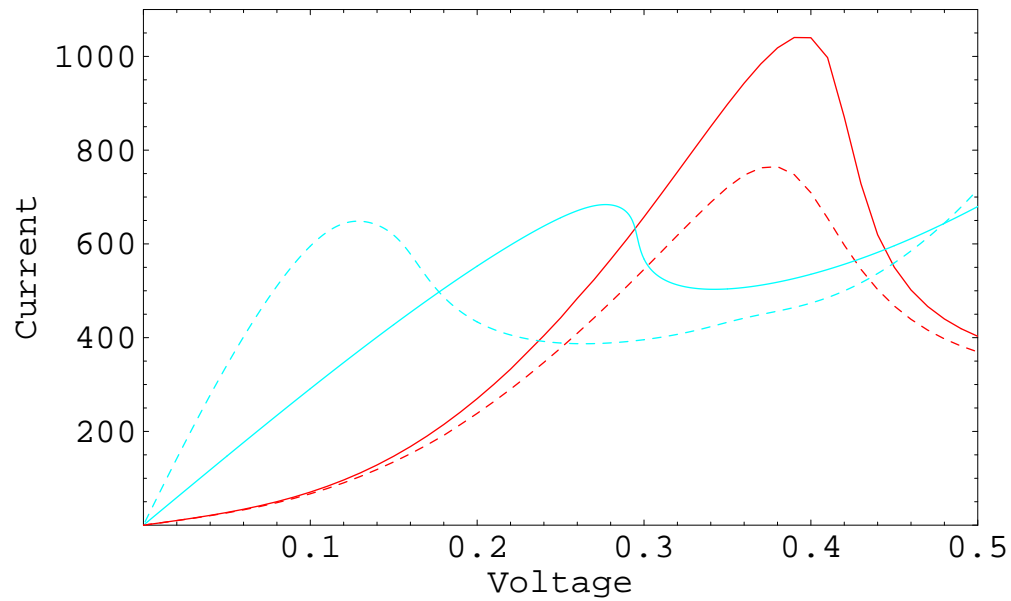


Figure 3: Current in kA/cm^2 vs. applied bias in volts for the thin (3.5 nm) well RTD: NEMO (red, dark), NEMO plus drift-diffusion (dotted red, dotted dark) in the contacts, smooth QHD with $\mu_{n0} = 1000 \text{ cm}^2/(\text{V s})$ (cyan, light) in the contacts, smooth QHD with $\mu_{n0} = 2000 \text{ cm}^2/(\text{V s})$ (dotted cyan, dotted light) in the contacts.

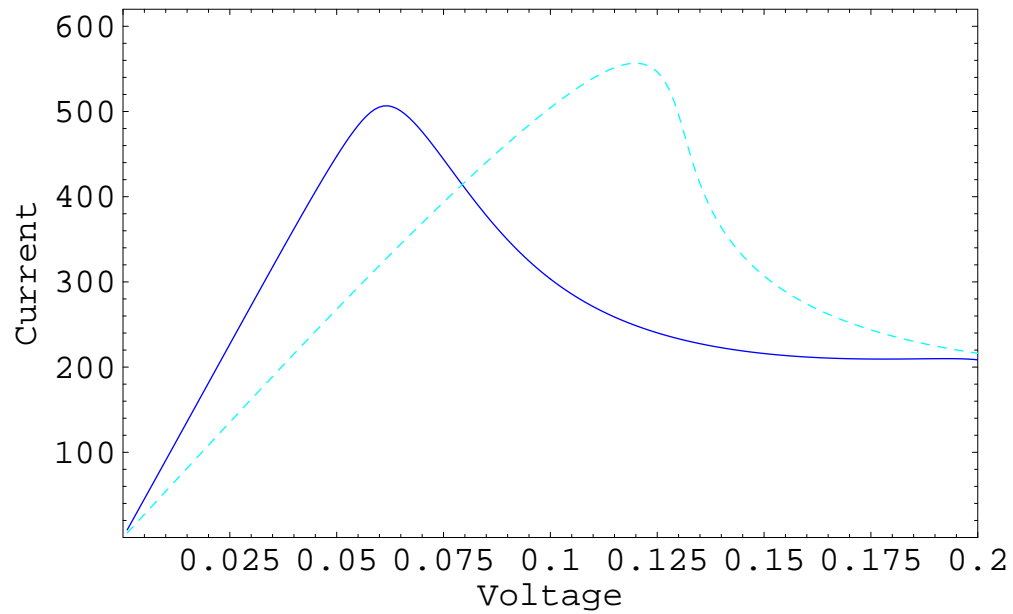


Figure 4: Current in kA/cm^2 vs. applied bias in volts for the medium well RTD: smooth QHD with constant $\tau_p = \tau_w$ (blue, dark) in the contacts, corresponding to a constant mobility $\mu_n = 2000 \text{ cm}^2/(\text{V s})$, compared with smooth QHD with $\mu_{n0} = 2000 \text{ cm}^2/(\text{V s})$ (dotted cyan, dotted light) in the contacts.

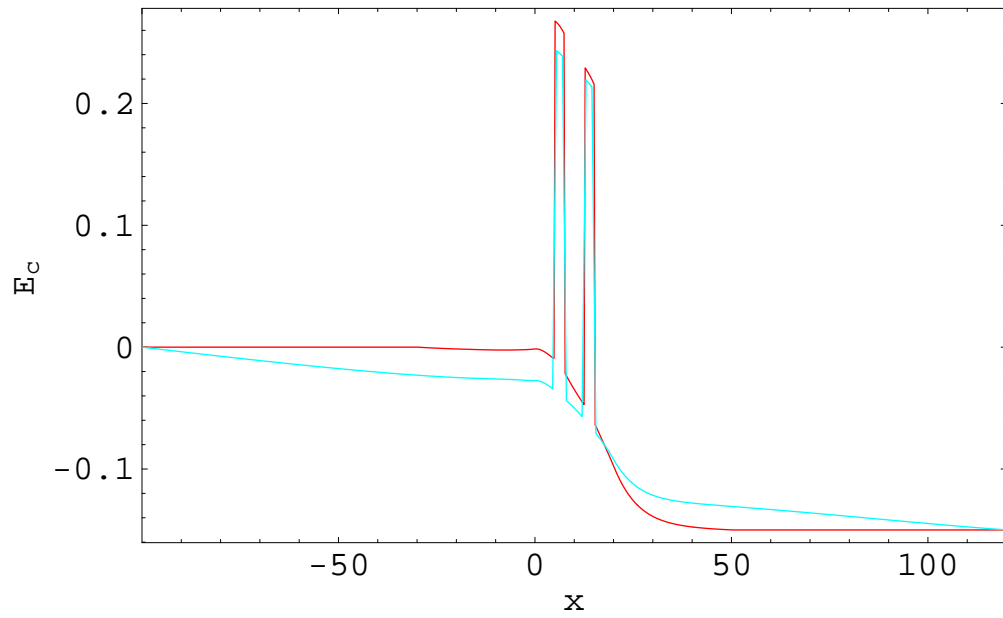


Figure 5: Conduction band energy E_c in eV vs. x in nm at $V = 0.15$ volts for the medium well RTD: for Figs. 5–10 NEMO (red, dark) with 30 nm contacts, smooth QHD with $\mu_{n0} = 1000 \text{ cm}^2/(\text{V s})$ (cyan, light) in the 100 nm long contacts.

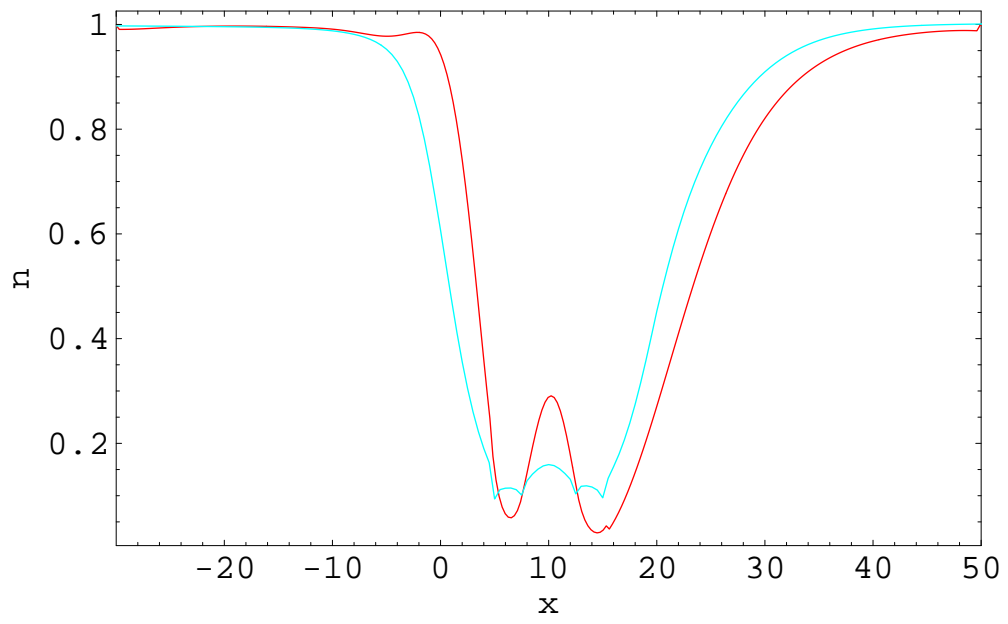


Figure 6: Electron density n in 10^{18} cm^{-3} vs. x in nm at $V = 0.15$ volts.

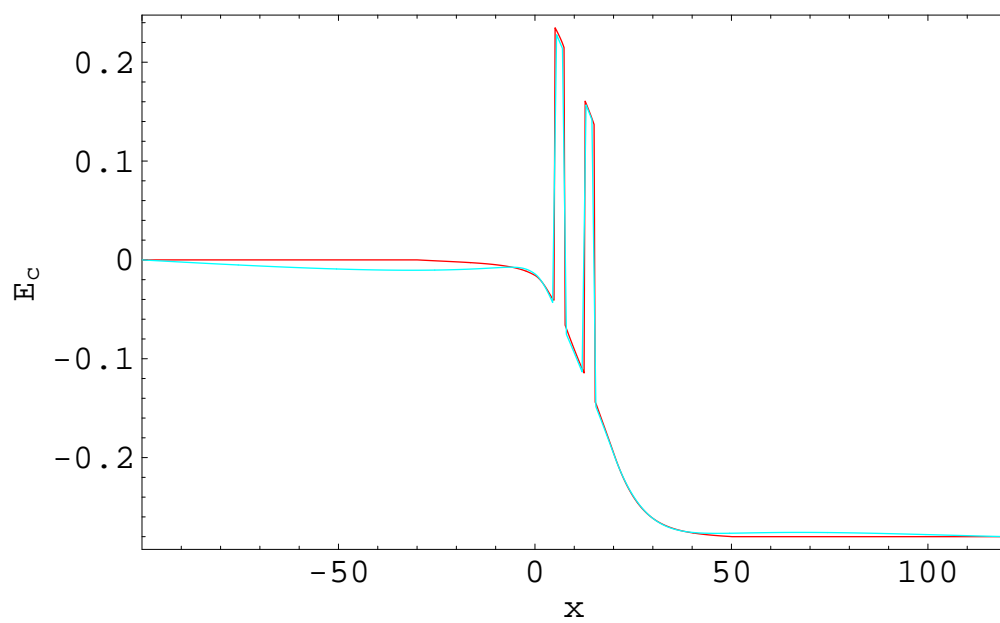


Figure 7: Conduction band energy E_c in eV vs. x in nm at $V = 0.28$ volts.

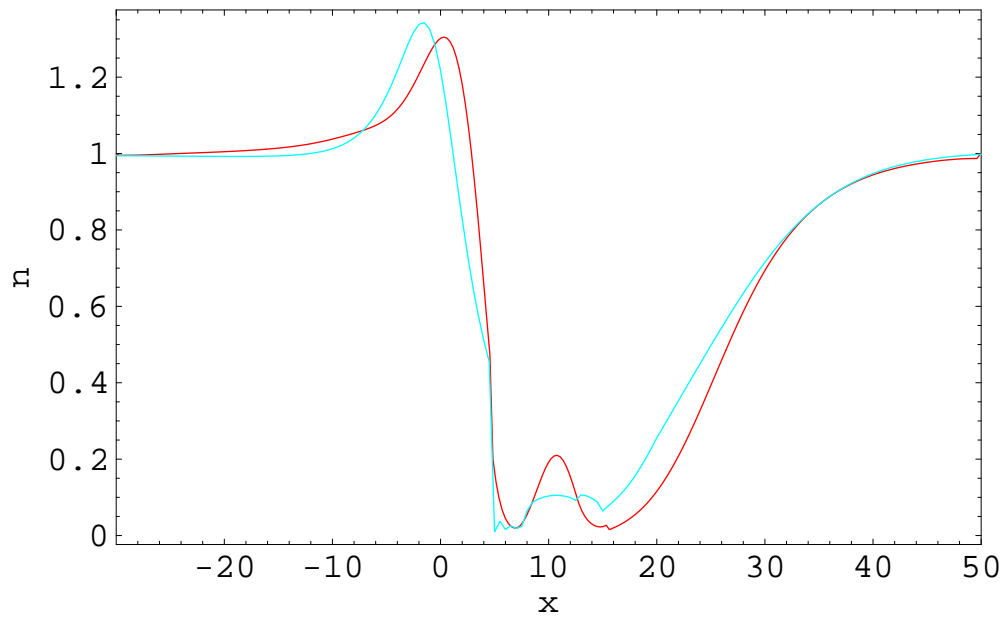


Figure 8: Electron density n in 10^{18} cm^{-3} vs. x in nm at $V = 0.28$ volts.

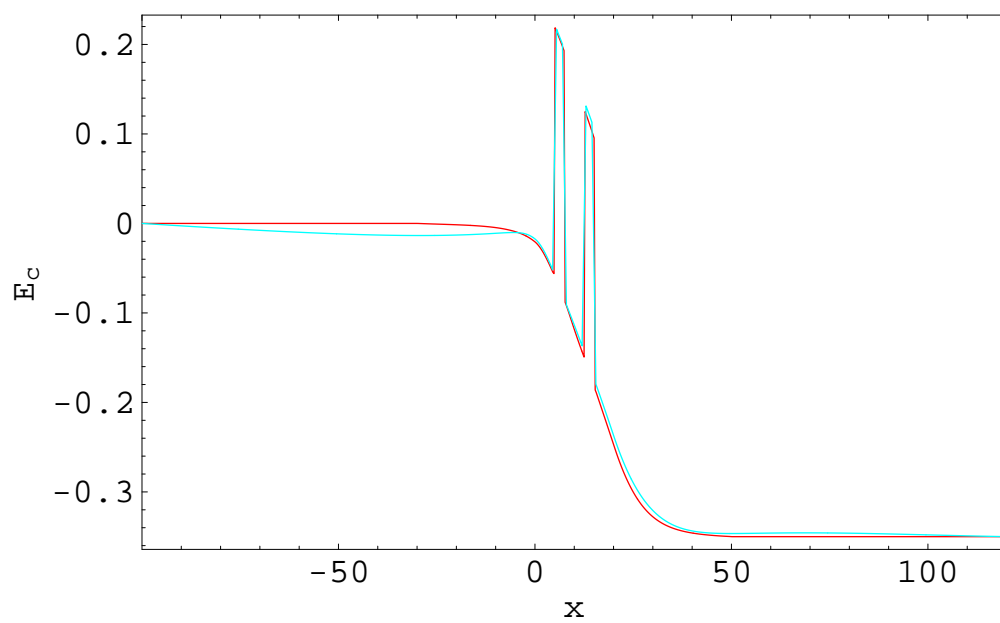


Figure 9: Conduction band energy E_c in eV vs. x in nm at $V = 0.35$ volts.

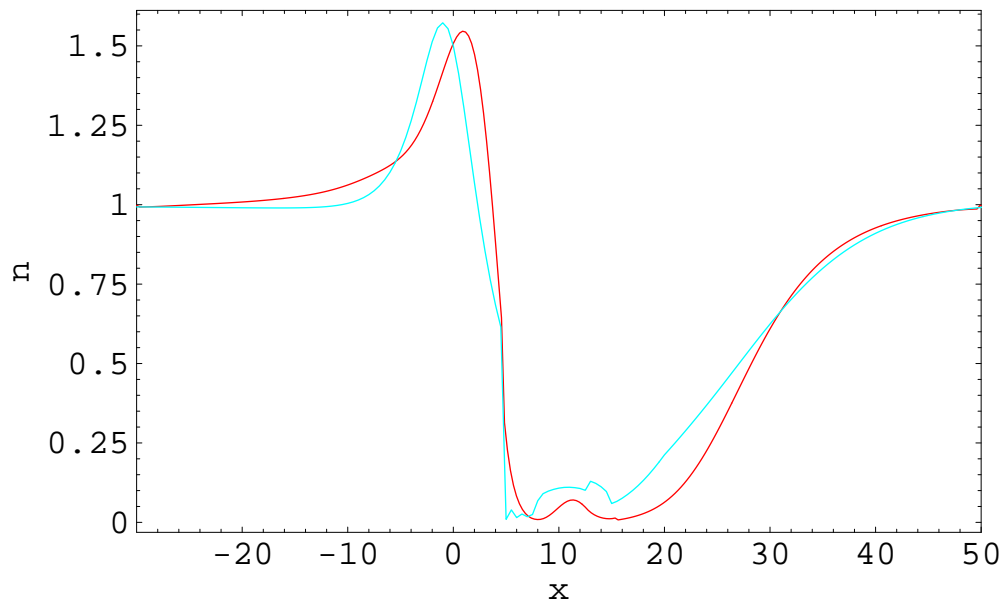


Figure 10: Electron density n in 10^{18} cm^{-3} vs. x in nm at $V = 0.35$ volts.

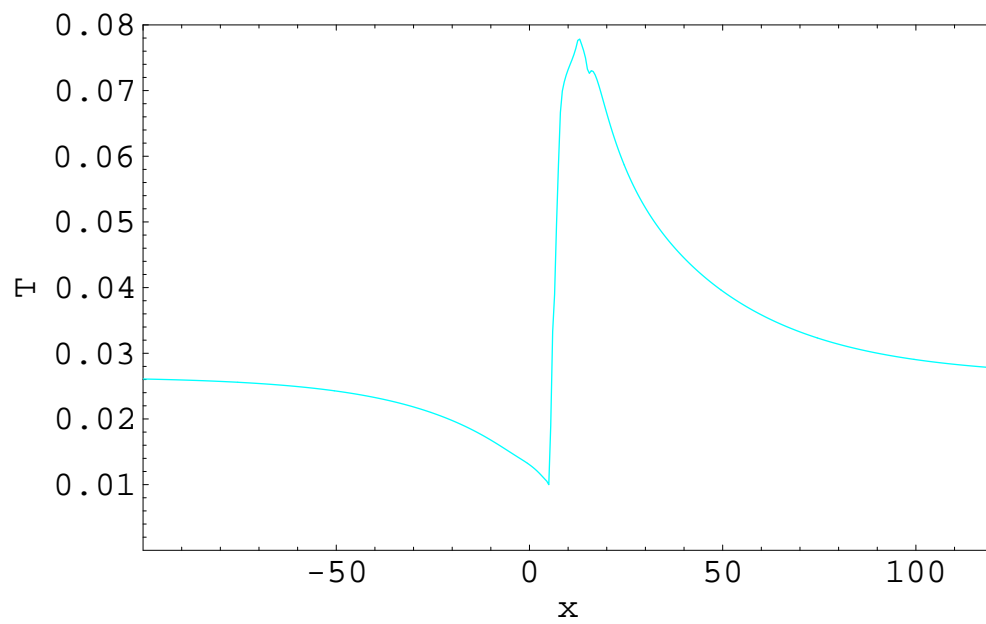


Figure 11: Electron temperature T in eV vs. x in nm at $V = 0.28$ volts for the medium well RTD: smooth QHD with $\mu_{n0} = 1000 \text{ cm}^2/(\text{V s})$ (cyan, light) in the contacts.